



1 **Geomorphic imprint of high mountain floods: Insight from the 2022**
2 **hydrological extreme across the Upper Indus terrain in NW Himalayas**

3 Abhishek kashyap¹, Kristen Cook², Mukunda Dev Behera^{1*},

4 ¹Centre for Ocean, River, Atmosphere and Land Sciences (CORAL), Indian Institute of
5 Technology Kharagpur, Kharagpur- 721302, West Bengal, India

6 ²ISTerre, Université Grenoble Alpes, 1381 Rue de la Piscine, 38610 Gières, France

7 **Emails:**

8 Abhishek Kashyap: kashyap95abhishek@kgpian.iitkgp.ac.in

9 Kristen L. Cook: kristen.cook@univ-grenoble-alpes.fr

10 (*Correspondence): Mukunda Dev Behera: mdbehera@coral.iitkgp.ac.in

11



12

13

14 **Abstract**

15 The interaction of tectonics, surface processes, and climate extremes impacts how the
16 landscape responds to extreme hydrological events. An anomalous precipitation event in 2022
17 occurred during the monsoon season along the lower reaches of the Upper Indus River,
18 resulting in short-lived high-magnitude flooding and socioeconomic disruption downstream.
19 To understand the spatial relationship between the geomorphic response and climatic controls
20 of this flood event, as well as their primary triggers, we performed a landscape analysis using
21 topographic metrics and quantified the causal association between hydro-climatic variables.
22 Temperature anomalies in upstream glaciated sub-catchments had a considerable impact on
23 snow cover distribution, based on our observations. As snow cover changed, glacial melt runoff
24 rose, contributing to increased fluvial stream power after traversing higher-order reaches. The
25 higher-order reaches of the Upper Indus River received an anomalously high amount of
26 precipitation, which, when combined with substantial glacial and melt discharge, contributed
27 to an extreme flood across the high-relief steep gradient channels. The flood-affected regions
28 had a high mean basin ksn and SL-index, including numerous spikes in their magnitudes along
29 their channel profiles downstream. To determine how the lower reaches of the Upper Indus
30 River responded to this flood event, we employed the Enhanced Vegetation Index (EVI) and
31 Normalized Difference Water Index (NDWI) as change indicator metrics. We observed an
32 inverse causal influence of NDWI on EVI and a statistically significant relationship between
33 anomalous stream power and relative EVI, suggesting that downstream channel morphology
34 changed rapidly during this episodic event and highlighting EVI as a useful indicator of
35 geomorphic change. We suggest that this extreme flood event is a result of the interaction of
36 anomalous glacial melt and anomalous precipitation over a high-relief landscape, with a certain
37 causal connection with anomalous temperature over the event duration. The synoptic
38 observations suggest that this meteorological condition involves the interaction of the Indian
39 Summer Monsoon (ISM) and Western Disturbance (WD) moisture fluxes. However, the
40 geomorphic consequences of such anomalous monsoon periods, as well as their influence on
41 long-term landscape change, are still unclear.

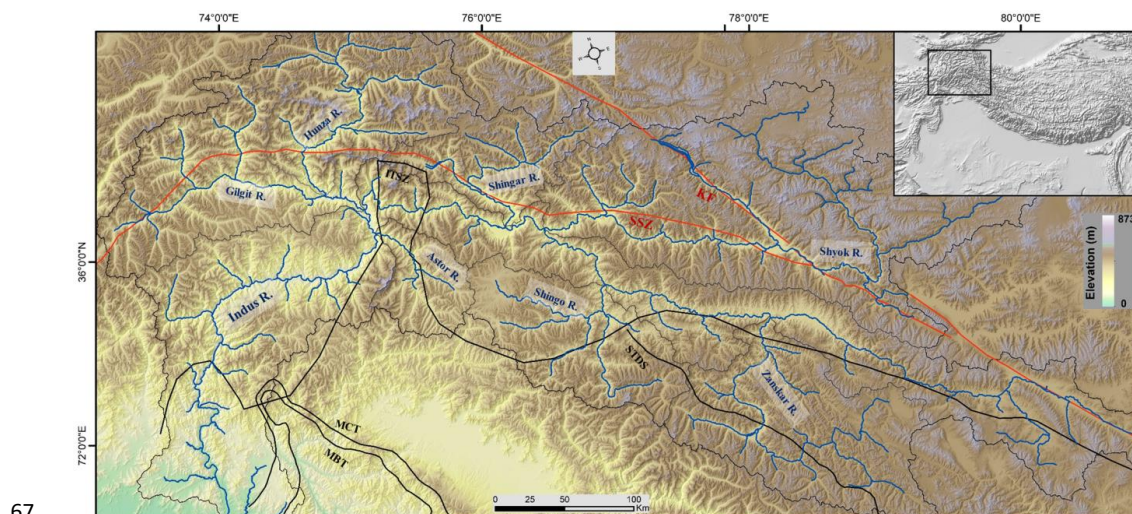
42 **Keywords:** anomalous precipitation; extreme flood; causal relationship; Upper Indus terrain



43 **1. Introduction**

44 High mountain floods in the Himalayas are associated with several processes, including
45 coupling of the Indian Summer Monsoon (ISM) and western disturbance (WD) circulations
46 (Houze et al., 2011), cloudbursts (Dimri et al., 2016), anomalous precipitation, cloud-scale
47 interconnected atmospheric anomalies (Dimri et al., 2017), and geomorphic driven surface
48 processes (Sharma et al., 2017). There is growing recognition that landscapes may evolve
49 through the cumulative effects of extreme episodic events, in particular in rapidly eroding
50 terrains (Korup, 2012; Cook et al., 2018). Recent studies suggest that even minor shifts in
51 weather patterns can have a significant impact on the frequency and magnitude of floods
52 (Knox, 2000; Liu et al., 2015; Benito et al., 2015; Sharma et al., 2022). It has also been
53 suggested that high-magnitude flood occurrences in the bedrock rivers draining the Himalayas
54 are the geomorphic agents with the most significant impact on the evolution of the regional
55 landscape as well as on the residents of the downstream regions (Bookhagen et al., 2005a;
56 Sharma et al., 2017; Panda et al., 2020).

57 The Tibetan Plateau and its surrounding mountainous regions, such as the Himalayas and the
58 Karakoram ranges, are critical for the downstream hydrology and water availability of the
59 Indus River system (Hewitt, 2009; Immerzeel et al. 2010) (Fig.1). The majority of the
60 hydrological budget of Indus River comes from precipitation, snowmelt, and glaciers, but their
61 relative contribution varies among the major contributing tributaries (Bookhagen and Burbank
62 2010; Wu et al., 2021). The Upper Indus catchment receives precipitation from two distinct
63 climatic systems, the WD and the ISM, over its foreland and highlands in the northwest
64 (NW) Himalayas (Bookhagen and Burbank 2006; 2010). However, it remains unclear yet how
65 these two distinct circulation patterns interact over the Himalayan landscape and what is their
66 potential influence on long-term geomorphic change (Dimri et al., 2015;2017; Ray et al., 2019).



67

68 Fig.1. Regional topographic setting of Upper Indus catchment along with its major tributaries
69 overlaid with major geological structures (MBT= Main boundary Thrust, MCT= Main Central
70 Thrust, STDS= Southern Tibet Detachment system, ITSZ= Indus Tibetan Suture Zone, SSZ=
71 Shyok Suture Zone, KF= Karakoram fault):

72 Short-duration episodic weather events have a significant influence on hillslope-surface
73 processes and rates of bedrock erosion by modulating mass movement and subsequent
74 landscape evolution (Snyder et al., 2003; Bookhagen et al., 2005b; Srivastava et al., 2017).
75 During such events, a lot of sediment is transported through the fluvial system, some of which
76 is temporarily deposited in low-gradient reaches and changes the landscape, before being
77 finally deposited in oceanic sinks (Goodbred, 2003; Panda et al., 2020). The geomorphic
78 signatures of catchment morphology are vital for understanding and identifying the channel
79 response involved in such events as well as the processes and patterns of erosion (Kashyap and
80 Behera., 2023; Sharma et al., 2017).

81 From the beginning of July until the end of August 2022, large portions of the Indus catchment
82 experienced unprecedented monsoon precipitation (Otto et al., 2023; Nanditha et al., 2023).
83 Some recent studies suggest that the primary trigger of this anomalous precipitation event was
84 an intensely low atmospheric circulation pattern, low sea surface temperatures across the
85 eastern Pacific, and the advent of a La-Nina event (Otto et al., 2023; Nanditha et al., 2023).
86 This extreme precipitation event resulted in a catastrophic flood in the low elevation flood
87 plains of the Indus catchment (Jones, 2022; Otto et al., 2023; Ma et al., 2023). This severe flood
88 had an extreme impact over the southern province of Pakistan, causing internal displacement



89 of about ~30–32 million people and the deaths of ~1500–1600 people (Bhutto, 2022; Khokhar,
90 2022; UNICEF, 2022; Ma et al., 2023). In excess of ~\$25–30 billion in economic losses are
91 anticipated (Bhutto, 2022; Otto et al., 2023). According to reports, the flood in 2022 exceeded
92 the peak flow rate of the disastrous 2010 floods that occurred over Pakistan (Bhutto, 2022;
93 UNICEF, 2022; Nanditha et al., 2023). The magnitude of the fluvial discharge over the
94 upstream tributaries of the Indus River increased predominantly as a result of increased
95 streamflow across glaciated channels (NDMA, 2022; UNICEF, 2022). However, the
96 geomorphic consequences and the main drivers of this high-magnitude flooding in the Upper
97 Indus catchment have not been evaluated yet.

98 In the present study, we evaluated the spatial distribution of channel changes in the
99 mountainous portion of the Upper Indus catchment due to the extreme precipitation event in
100 the months of July and August 2022. We employed a channel slope-discharge product along
101 the trunk channel of the Upper Indus River to estimate the anomalies in the stream power
102 resulting from the anomalous precipitation event during July and August 2022. We used a
103 random-forest-based machine learning approach to compare the observed and predicted
104 intensity of precipitation and runoff by assessing the mean climatology of independent hydro-
105 climatic variables. We further quantified the causal relationship between hydro-climatic drivers
106 using nonlinear time series data over the event duration. We investigated the channel response
107 of this episodic flood event by using the NDWI and EVI as change indicator metrics and
108 comparing that to event characteristics such as anomalous precipitation, stream power, and
109 channel metrics. We want to better understand the controls on where and when these types of
110 extreme hydrological events will substantially modify rivers and landscapes so associated
111 geomorphic hazards can be better anticipated, and we also want to better constrain the potential
112 role of these episodic events in driving long-term geomorphic change across the western
113 syntaxial region.

114 **2. Regional Setting**

115 In the Himalayas, the erosion rates are high and the landscape of the mountainous terrain is
116 shaped by the interactions between river systems and the basement tectonics (Jaiswara et al.,
117 2019; 2020). Among the Himalayan River systems, the Upper Indus is unique, including a fully
118 developed, ~1200-1400 km long, 8th- 9th-order drainage that enters the Himalayan terrain as an
119 antecedent channel and cuts right over the seismically active belt in the Indus- gorges (Fig. 1).
120 This catchment is highly affected by recurrent landslides or debris flows, and episodic glacial



121 and landslide dams that represent significant geomorphic hazards (Korup & Montgomery
122 2008; Korup et al., 2010).

123 The Upper Indus River flows through the highly tectonically active region of the Nanga
124 Parbat-Haramosh Massif (NP-HM), which is one of the highest relief regions on earth (~>5000
125 m), and has the strong potential to rapidly erode uplifted material (Leland et al. 1998; Shehzad
126 et al. 2009; Korup et al. 2010). The NP-HM region experiences the highest recorded rates of
127 denudation and channel incision on earth (~12 mm/y), as well as high rates of tectonic uplift
128 (~4 -10 mm/y) and forms river anticlines across extremely weak crust (Koons et al., 2002;
129 2013; Zeitler et al., 2001; 2014; Butler, 2019). This has a significant impact on the tectonics
130 and morphology of the western Himalayas (Hewitt, 2009; Zeitler et al., 2014). The Upper Indus
131 catchment (UIC) is characterized by extremely steep channel gradient of ~>20-25°, high
132 topographic relief of ~4000–5000 m, and a large portion of snow covered peaks (Hewitt, 2007;
133 Farinotti et al., 2020).

134 As a fraction of the total annual discharge, snowmelt constitutes up to 50% in the
135 Upper-Indus catchment (UIC) (Burbank & Bookhagen, 2006; 2010; Scherler et al., 2011). Due
136 to the Western Disturbance (WD) inclination, the UIC has a lot of precipitation in the winter
137 and spring (Kapnick et al., 2014), while due to the orographic barrier of the high mountains,
138 the influence of the ISM in the region weakens towards to the north-west (Forsythe et al., 2017).
139 The annual precipitation in the UIC increases with the elevation; across the northern valley
140 floors- in the rain shadows it ranges from 100-200 mm/y; while at elevation ~4000-4400
141 ma.s.l., it ranges from 600-800 mm/y; and above >~5000 ma.s.l., it ranges from 1500 -2000
142 mm/y (Sharif et al., 2013; Wu et al., 2021). From October to March, the monthly mean
143 temperatures in the UIC are below freezing at elevations > ~3000 m (Archer, 2004). Discharge
144 in the tributary channels of the Upper Indus River that depend on glacier meltwater has a strong
145 association with summer time mean air temperatures across the Karakoram ranges (Forsythe
146 et al., 2017; Wu et al., 2021).

147 **3. Materials and Methodology**

148 **3.1 Data Used**

149 In the present study, we used a 30 m SRTM digital elevation model (DEM) for landscape
150 characterization and geomorphic quantitative parameter estimation. In order to investigate how
151 the climatic variables driving this extreme event affect the processes of regional erosion, we



152 used 40 years' (1982–2022) duration of daily precipitation datasets from the July 1 to August
153 31 period from CHIRPS (Climate Hazards Group Infrared Precipitation with Station Data)
154 (Version 2.0 Final). Using the climatology of daily datasets from July 1 to August 31, we
155 observed the spatiotemporal occurrence of hydro-meteorological variables. These variables
156 included 2-m air temperature, skin temperature, dewpoint temperature, snowmelt, and runoff
157 acquired from ERA5-Land Daily Aggregated-ECMWF Climate Reanalysis with a spatial
158 resolution of 11132 meters. We used remote sensing-based indices, such as MODIS-derived
159 normalized difference water index (NDWI), normalized difference snow index (NDSI), snow
160 albedo, EVI, and surface reflectance bands b1 and b2, with a spatial resolution of 500 meters,
161 for anomalous change indicators.

162 **3.2 Drainage network extraction and landscape analysis.**

163 We extracted the drainage network from the DEM using the ArcGIS platform. A regional slope
164 map was produced by running a 1000 m radius mean filter over the slope model derived from
165 the DEM, and a regional relief map was generated by passing a 1000 m circular radius focal
166 range window over the DEM. Further analysis of the DEM and the derived flow accumulation
167 data were performed in MATLAB using the transient profiler tools (Jaiswara et al., 2019,
168 2020). We extracted the longitudinal profiles of the bedrock channels within an accumulation
169 region of about 1×10^6 m² and channel network of the Upper Indus catchment using
170 TopoToolbox (Wobus et al., 2006; Kirby and Whipple, 2012; Schwanghart and Scherler,
171 2014). We used a 1000 m smoothing window and a 20 m vertical interval to sample the channel
172 networks in order to reduce the noise and artefacts that are embedded in the elevation data.

173 **3.3 Quantitative Geomorphic parameters**

174 We used geomorphic quantitative parameters such as SL (Stream length-gradient index)-index,
175 k_{sn} (Normalized steepness index) and Stream power of the Upper Indus trunk channel to
176 evaluate the influence of the high magnitude flooding event across the Upper Indus River
177 during July and August 2022. To evaluate the spatial variability of the flood magnitude and the
178 channel morphology, these metrics are plotted on the longitudinal profile of the trunk channel.

179 **3.3.1 Stream length-gradient index (SL- Index)**

180 Rivers often achieve an equilibrium or steady state between erosion and sedimentation, which
181 is represented by a concave longitudinal river profile (Schumm et al., 2002). Tectonic,
182 lithological, and/or climatic factors often result in shifts in river profiles from this expected



183 steady-state condition (Hack, 1973; Burbank and Anderson, 2011). Here, we use the Stream
184 Length-Gradient (SL) index to identify the zones of topographic break and changes in the
185 channel gradient of the longitudinal profile by using the equation:

186
$$SL = (\Delta H/\Delta L)/L \dots \dots \dots (1)$$

187 where SL denotes the steepness or gradient of the profile for the local reach, L is the total river
188 length from the midpoint of the local reach to the highest point on the channel, ΔH is the change
189 in elevation over the reach and ΔL is the length of the reach, so $\Delta H/\Delta L$ represent the channel
190 slope or gradient of the reach. A sharp lithological variation and/or the differential uplift across
191 active structures are frequently linked to an abrupt change in SL-index along the river (Hack,
192 1973; Jaiswara et al., 2020; Kashyap et al., 2024).

193 **3.3.2 Channel Steepness index**

194 We extracted the bedrock profile of the Upper Indus River, which can be described using the
195 power law relationship between upstream drainage area (A) and channel gradient (S) as
196 (Jaiswara et al., 2019, 2020; Kashyap et al., 2024):

197
$$S = k_s A^{-\theta} \dots \dots \dots (2)$$

198 where $k_s = (E/K)^{1/n}$ is the channel steepness index, $\theta = (m/n)$ is the channel concavity index,
199 m and n are positive constants, E is the erosion rate at a steady state (Wobus et al., 2006; Kirby
200 and Whipple, 2012). The relative magnitude of k_s is often related to the surface uplift rate as
201 well as the erosional efficiency across a bedrock catchment (Snyder et al., 2003; Wobus et al.,
202 2006).

203

204 **3.3.3 Stream Power estimation**

205 The normalized steepness index (k_{sn}) has emerged as an important topographic metric with
206 significant correlation with erosion rate over a wide range of timescales (Wobus et al., 2006;
207 Jaiswara et al., 2019; Kashyap et al., 2024). However, one major drawback of k_{sn} is that it
208 includes an assumption of spatially constant precipitation because upstream drainage area is
209 used as a proxy for discharge (Adams et al., 2020; Leonard et al., 2023a).

210 In the present study, we incorporate the precipitation intensity into the stream power law
211 to analyze the anomalous stream power along the trunk channel during the flood event. We



212 estimate the precipitation induced stream power using the slope-discharge method, which
213 involves multiplying the accumulated flow distance weighted by precipitation with the
214 hyperbolic tangent function of the channel gradient along the flow path (Adams et al., 2020;
215 Leonard et al., 2023b). The estimation of stream power ($K_{sn}Q$) as a function of channel
216 discharge can be estimated as:

$$217 \quad K_{sn}Q = (S) \times f(\int p * FD) \dots\dots\dots (3)$$

218 where S is the channel gradient, FD is the accumulated flow distance, p is the accumulated
219 precipitation (Leonard et al., 2023a; b). Thus, $K_{sn}Q$ is a normalized version of the channel
220 steepness metric that uses the product of channel gradient (S) and upstream discharge (Q)
221 estimated from mean precipitation (P) as a fluvial discharge proxy. This enables $K_{sn}Q$ to
222 account for the spatial and temporal variability in precipitation along the upper Indus River
223 during the high magnitude flood event. Accumulated precipitation resolves spatial patterns well
224 and scales nearly linearly with relevant discharges, particularly for large and long-lasting
225 precipitation events (Rossi et al., 2016; Leonard et al., 2023a; b).

226 **3.4 Machine learning based approach to model the anomalous event characteristics**

227 The Random Forest (RF) technique is a supervised machine learning method that has been used
228 as a tree-based ensemble technique and includes a bagging or boot-strapping algorithm
229 (Breiman, 2001; Wolfensberger et al., 2021). In the present study we use a RF based
230 multivariate regression approach to estimate the anomalous precipitation and runoff intensity
231 in July and August 2022 using the independent variables obtained from classifying variable
232 importance.

$$233 \quad H(x) = \sum_{i=1}^T h_i(x) \dots\dots\dots (4)$$

234 Where, $h_i(x)$ denotes the i^{th} regression tree output (h_i) on sample x. Therefore, the prediction
235 of the RF is the mean of the predicted values of all the decision trees. T denotes the regression
236 trees for regression prediction.

237 Based on the mean climatology of the last 40 years, we predict the daily anomalous
238 precipitation and runoff intensity for the 2022 event and compare them with the observed actual
239 values. We employed the highest significance variables, as well as precipitation and runoff data
240 from 1982 to 2021, as a training set. To utilize the independent variables to estimate these event
241 characteristics, we first classify the hydro-climatic variables based on their higher importance



242 using the RF classification approach. Then, using the RF multivariate regression approach, we
243 select only those independent variables with the highest significance to estimate anomalous
244 precipitation and runoff intensity during the event duration.

245 **3.5 Causal discovery among Hydro-climatic variables**

246 Causal methodologies have been utilized to evaluate whether and how changes in one hydro-
247 climatological variable during anomalous extreme events influence the magnitude of another
248 (Runge et al., 2019a; Nowak et al., 2020). To understand how an extreme event is regulated
249 over high mountainous terrain, a temporal investigation of event characteristics is required.
250 Using this evaluation, we gain insight into how the conditioning hydro-climatic variables that
251 regulate these extreme events evolve throughout event duration in a catchment (Runge, 2018;
252 Krich et al., 2020). Understanding directional dependencies is crucial to distinguish them from
253 connections that cannot be deduced using any statistical model (Kretschmer et al., 2017;
254 Karmouche et al., 2023).

255 In this study, we use causal stationarity, and the absence of contemporaneous causal effects
256 for the time series datasets using the PCMCI and MCI approaches (Tibau et al., 2022; Runge,
257 2023). PCMCI is a causal identification technique that combines the Momentary Conditional
258 Independence (MCI) approach with the PC algorithm (Runge et al., 2019b; Nowack et al.,
259 2020). Given a set of multivariate time series, PCMCI estimates the time series graph that
260 depicts the conditional independencies among the time-lagged factors (Runge et al., 2014;
261 2019a). In addition to PCMCI, we use the ParCorr linear independence test based on partial
262 correlations is employed (Runge et al., 2014; 2023).

263 In the present study we use the daily datasets of hydro-climatological variables and group
264 them as; Temperature gradient (Tg), including Air temperature, Surface temperature, and
265 Dewpoint temperature; Rainfall gradients (Rg), including Precipitation intensity, Runoff and
266 Snowmelt; and anomalous change indicators (Ac) including EVI, NDWI, and NDSI, July 1 to
267 August 31, 2022, so includes 62 observational intervals. We evaluate the causal interference
268 between these hydro-climatic variables using the MCI approach with a maximum 2-day lag
269 period ($\tau_{\max} = 2$) and a limit for significance set to 0.05 ($\alpha = 0.05$), in order to examine the
270 spatially interdependence relationships among each of these variables during 2-day event
271 periods.

272 **3.6 Moisture pathways**

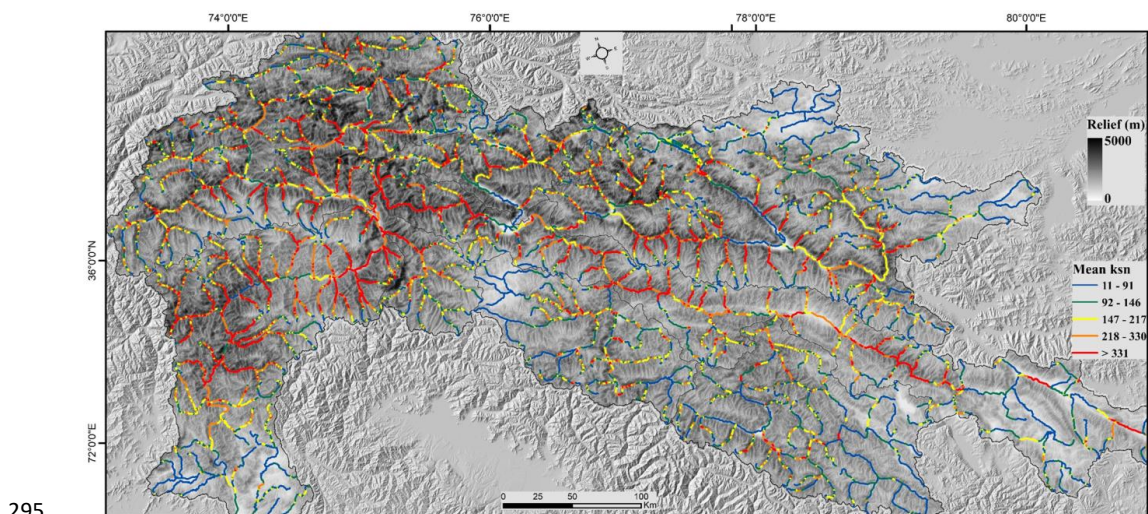


273 The Hybrid Single-Particle Lagrangian Integrated Trajectories (HYSPLIT) model
274 (https://www.ready.noaa.gov/HYSPLIT_traj.php) has been employed to determine the
275 probable moisture parcel source region (Joshi et al., 2023). Over the past decade, researchers
276 have used the HYSPLIT model to identify moisture sources (Wang et al., 2017; Joshi et al.,
277 2023). To determine the backward trajectory following an anomalous precipitation event, this
278 study used the HYSPLIT model. We used three starting heights of 500, 1000, and 3000 m a. s.l
279 to calculate the backward trajectory for each day of July and August 2022, given that the
280 HYSPLIT model required the start date/time, location, and height for each precipitation event
281 (Wang et al., 2017; Gudipati et al., 2022). This study used meteorological data with a spatial
282 resolution of $1^{\circ} \times 1^{\circ}$ from the Global Data Assimilation System (NCEP-GDAS).

283 **4. Results**

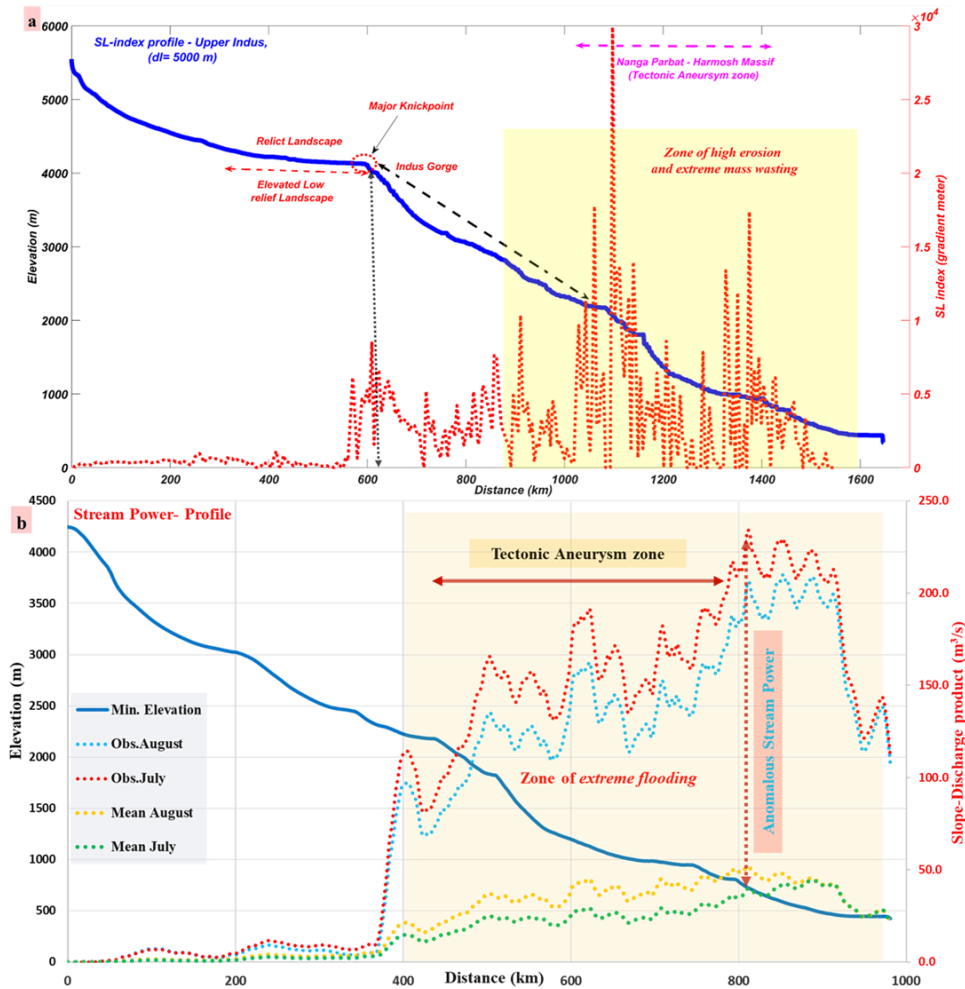
284 **4.1 Geomorphic analysis of the Upper Indus terrain**

285 The Indus River is around ~1400–1600 km long and forms multiple loops both parallel to and
286 in opposition to the regional structural trend; its bed elevation ranges from ~500–6000 m. The
287 river exhibits distinct morphological characteristics over its flow path in terms of its
288 topographic attributes and derivatives. Over the elevated low-relief landscape in the Tibetan
289 plateau, the relief and channel gradient vary as (~0–500 m; ~0–10°), with a low SL index (~ 1
290 $\times 10^4</math> gradient meter and mean basin k_{sn} of (~90 $m^{0.9}</math>) (Fig. 2; Fig. 3a). Then, when the river
291 traverses through the NP-HM region, there is a progressive rise in the local relief and channel
292 gradient to (~>2000–3000 m; ~>25–35°), which is also reflected in the SL-index (>2.5–3 $\times 10^4</math>)
293 and mean k_{sn} (~>331 $m^{0.9}</math>). This region is characterized by topographic discontinuities across
294 active structures, leading to high relief variation and topographic roughness.$$$$



296 Fig.2. Spatial distribution of local relief overlaid with Mean basin ksn ranges across the Upper
297 Indus River catchment.

298 The tributaries in the upstream glaciated valleys that flow parallel to the structural trend
299 have a higher mean channel gradient ($> \sim 20\text{-}30^\circ$) and topographic relief ($> \sim 2000\text{-}3000$ m) (Fig.
300 2). When these tributary channels start to descend towards the main stream after following the
301 glaciated landscape, the value of SL and k_{sn} for the trunk channels shows a significant rise at
302 $\sim 3000\text{-}4000$ m mean elevation. Approaching the southern mountain front, the main trunk
303 channel relief and channel gradient are $\sim 1000\text{-}2000$ m and $\sim 15\text{-}25^\circ$ respectively (Fig. 3a).



304

305 Fig.3. The trunk channel profile of Upper Indus river plotted with (a) SL-index; (b) The highest
306 order profile of Upper Indus river plotted with Stream power (slope-discharge product)-channel
307 elevation (highest order profile is the subset of trunk channel profile indicated by black dash
308 line).

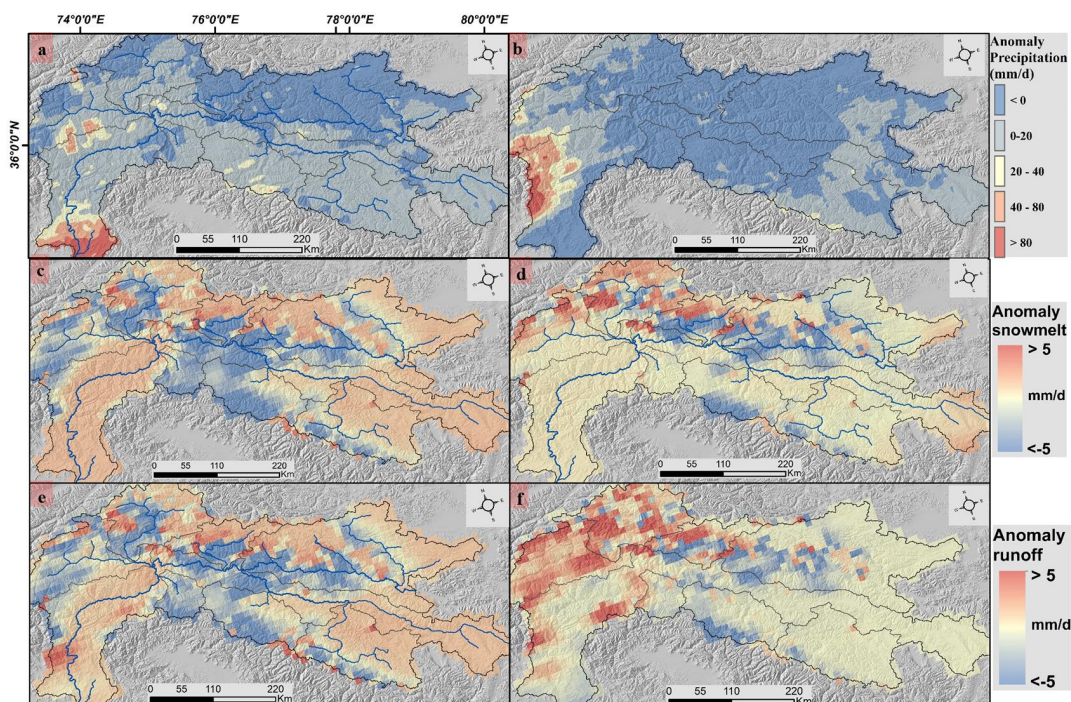
309 The spatial association of higher k_{sn} ($>\sim 331 \text{ m}^{0.9}$), topographic relief ($\sim 1500\text{-}2000 \text{ m}$),
310 and longitudinal increase in channel gradient along the main Upper Indus River channel
311 downstream suggests a higher erosional regime. These high values for the various topographic
312 metrics highlight zones of accelerated erosion where the river is in gradational disequilibrium.
313 Furthermore, this tectonically active southern front coincides with a region that gets significant



314 annual mean precipitation (~1500–2500 mm/y), suggesting a tectonic-climate linkage in the
315 erosional process.

316 **4.2 Spatial distribution of Hydro-climatic anomalies over event duration**

317 The downstream reach of the Upper Indus trunk channel received significant amount of
318 anomalous precipitation (>~60–80 mm/d) during the observation period of July and August
319 2022 (Fig. 4a, 4b). The spatial variability of anomalous precipitation varies with a range of
320 >~0–40 mm/d along its major glaciated tributaries, such as Hunza, Astor, Gilgit, Shingo, and
321 Zaskar. In July and August 2022, the total extent of anomalous precipitation was around
322 ~900–1000 mm/month, which was approximately ~300–400% more than the long-term (1982–
323 2022) mean climatology. From July to August 2022, there was continuous precipitation in the
324 high gradient downstream region, and due to the antecedent weather conditions, extreme
325 precipitation likely produced suitable conditions for high-magnitude flooding. The potential
326 geomorphic response of such anomalous precipitation is suggested by the resulting anomalous
327 stream power over the downstream channels (Fig. 4c, 4d). The spatial distribution of
328 anomalous stream power shows that the greatest increase occurred at ~400–800 km along the
329 channel profile downstream. For both the months of July and August of 2022, we observed a
330 significant rise in the stream power, to ~>200 m³/s above the mean values (Fig. 3b).



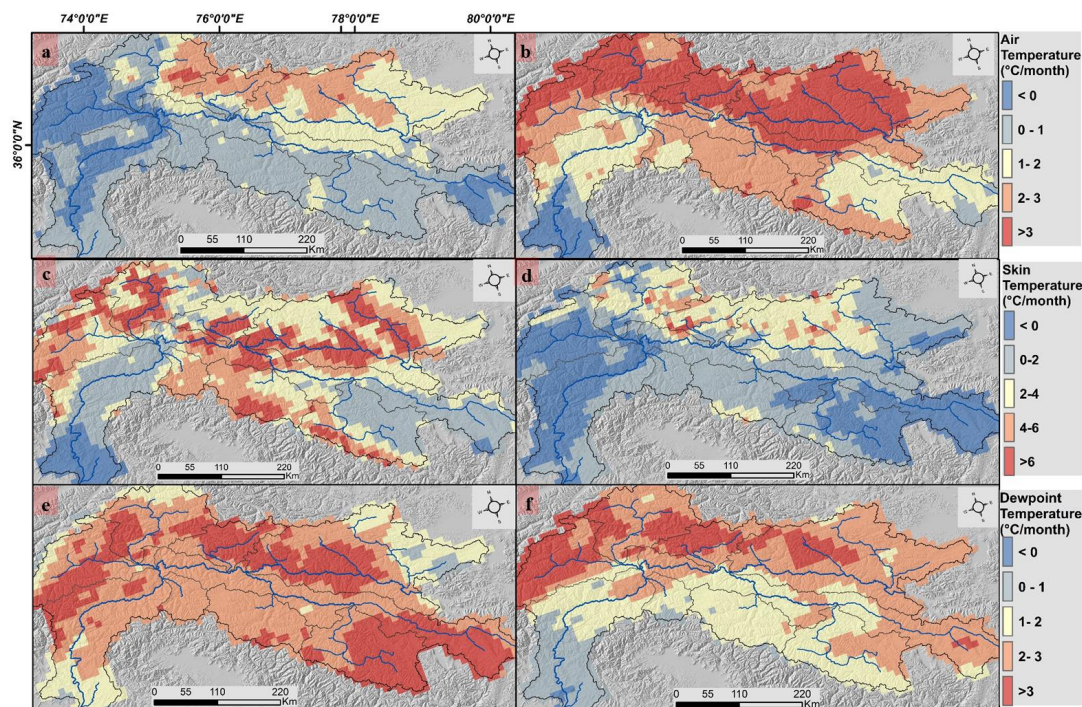
331

332 Fig.4 Spatial distribution of hydro-meteorological variables for anomalous July and August
 333 month of 2022 across Upper Indus catchment such as: (a) precipitation (July) (b) precipitation
 334 (August) (c) Snowmelt (July) (d) snowmelt (August); (e) Runoff (July) (f) Runoff (August).

335 During the observation period, other variables, such as runoff and snowmelt, also showed
 336 positive anomalies across the upstream glaciated sub-catchments over the Karakoram ranges
 337 (Fig. 4e, 4f). Furthermore, during July and August 2022, the temperature variables indicated a
 338 positive deviation from the mean climatological trend over the glaciated catchments. In the
 339 upstream sub-catchments in Shyok, Shingar, Hunza, and Gilgit, air and dewpoint temperatures
 340 reach ($> \sim 3^{\circ}\text{C}$ above mean), while surface temperatures reach ($> \sim 6^{\circ}\text{C}$ above mean) (Fig. 5).
 341 The spatial distribution of anomalous temperatures corresponds well with the anomalous
 342 snowmelt and runoff magnitude across the upstream glaciated catchments.



343



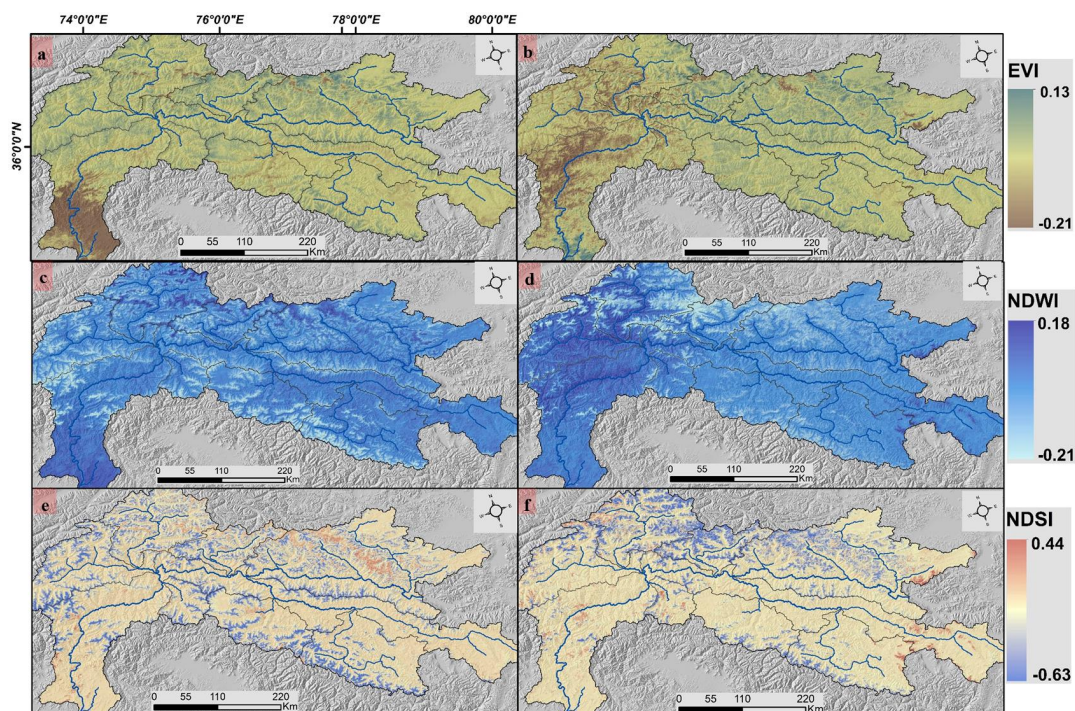
344

345 Fig.5 Spatial distribution of hydro-meteorological variables for anomalous July and August
 346 month of 2022 across Upper Indus catchment such as: (a) Air temperature (July) (b) Air
 347 temperature (August) (c) Surface temperature (July) (d) Surface temperature (August); (e)
 348 Dewpoint temperature (July) (f) Dewpoint temperature (August).

349 We also observed a significant shift in the spatial distribution of change indicator
 350 variables during the observation period. In July 2022, the lower reaches of the Upper Indus
 351 River exhibited a negative change in EVI (~ -0.21) and a positive relative NDWI ($\sim 0.15-0.20$).
 352 This inverse relationship between these two change indicators was found in the upstream
 353 channel as well in August. During the event, the tributary channels in the upstream glaciated
 354 landscape experienced a significant change in snow cover distribution, as demonstrated by the
 355 spatial variations of the relative NDSI ($\sim 0-0.63$). Changes in relative snow cover correspond
 356 directly to increases in snowmelt and glacial runoff across glaciated catchments (Fig. 6). We
 357 observed a significant relationship ($p < 0.005$; $R = 0.81$) between the relative EVI metric and the
 358 anomalous stream power in the Upper Indus trunk channel and along its main tributaries. The
 359 anomalous stream power of the Upper Indus River and all of its major tributaries corresponds
 360 to a proportion of EVI change that exceeds across low-gradient regions. This positive

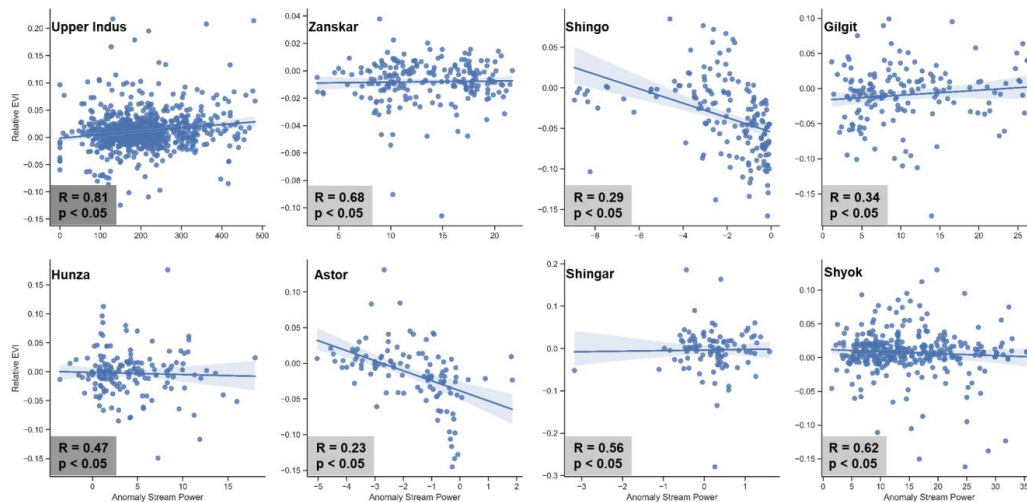


361 relationship with an increasing trend suggests a substantial geomorphic response due to
362 extreme flooding. However, a negative relationship between anomalous stream power and EVI
363 can also be observed across the channels of Astor and Shingo (Fig. 7).



364

365 Fig. 6. Spatial distribution of hydro-meteorological variables for anomalous July and August
366 month of 2022 across Upper Indus catchment such as: (a) EVI (July) (b) EVI (August) (c)
367 NDWI (July) (d) NDWI (August); (e) NDSI (July) (f) NDSI (August).



368

369 Fig.7. Statistical relationship between Relative EVI- Anomalous Stream Power from July 1 to
 370 August 31, 2022 across Upper Indus catchment as well as along its all the major tributaries:

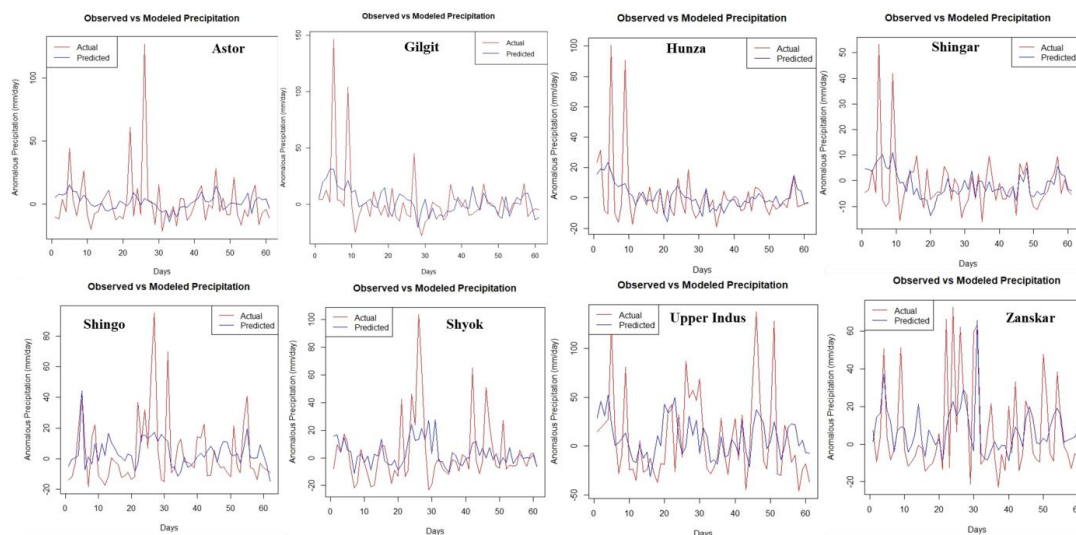
371 **4.3 Machine learning based approach to quantify the event anomalies**

372 The RF-classification-based determination of variable importance indicates that dewpoint
 373 temperature is the most significant variable in estimating precipitation intensity. Other
 374 significant variables include surface temperature and air temperature. Relative NDSI was the
 375 variable of highest significance for estimating precipitation in all other sub-catchments except
 376 Shingar (Fig. S1). Snowmelt, dewpoint temperature, relative NDSI, and surface temperature
 377 are the most significant variables for each sub-catchment when estimating runoff intensity.
 378 Surface temperature holds higher significance in the trunk channel catchment of the Upper
 379 Indus, followed by air temperature and precipitation intensity (Fig. S2). The anomalous
 380 precipitation and runoff intensity are then estimated using these independent variables with the
 381 highest significance obtained during classification.

382 The results show that the Upper Indus catchment received significantly more
 383 precipitation and runoff than predicted at multiple instances in July and August of 2022 (Fig.
 384 8). The anomalous and extreme characteristics of the hydro-climatic and terrestrial drivers
 385 could explain this phenomenon. The Upper Indus catchment received a significant amount of
 386 anomalous precipitation, with an intensity of >~100 mm/d, which is much higher than the
 387 predicted intensity during the period of observation. The channels in the higher relief
 388 landscapes such as Astor and Gilgit encountered the second-highest anomalous incidence, with



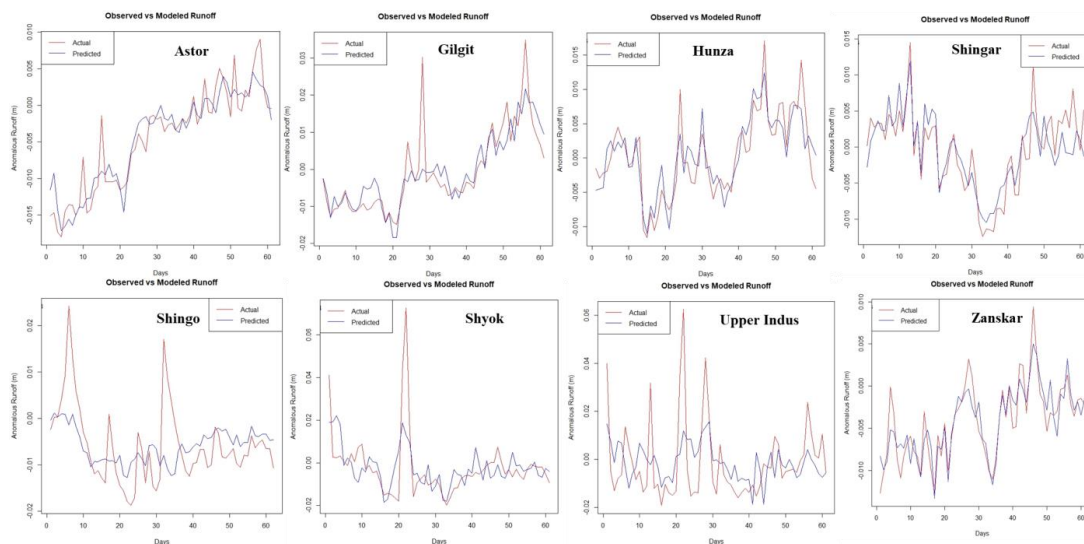
389 intensities ~80–100 mm/d. The upstream glaciated catchments, such as the Shyok, Shingo, and
390 Hunza, also have persistent anomalous intensities of up to ~100 mm/d. The least impacted
391 catchment was Zanskar and Shingo, despite a high rate of precipitation that ranges from ~60–
392 80 mm/d.



393

394 Fig.8 Random Forest-Regression based observed vs modeled anomalous precipitation from
395 July 1 to August 31, 2022 across Upper Indus catchment as well as along all the major
396 tributaries.

397 The distribution of observed and predicted runoff shows the intensity of observed runoff
398 corresponds with the precipitation trend. During the observation period, the Upper Indus
399 catchment had much higher runoff rates, followed by upstream glaciated sub-catchments
400 including Shyok (~30-60 mm/d), Shingo, and Gilgit (~20-30 mm/d). However, in the majority
401 of the upstream sub-catchments, the observed anomalous runoff intensity is insignificant (Fig.
402 9).



403

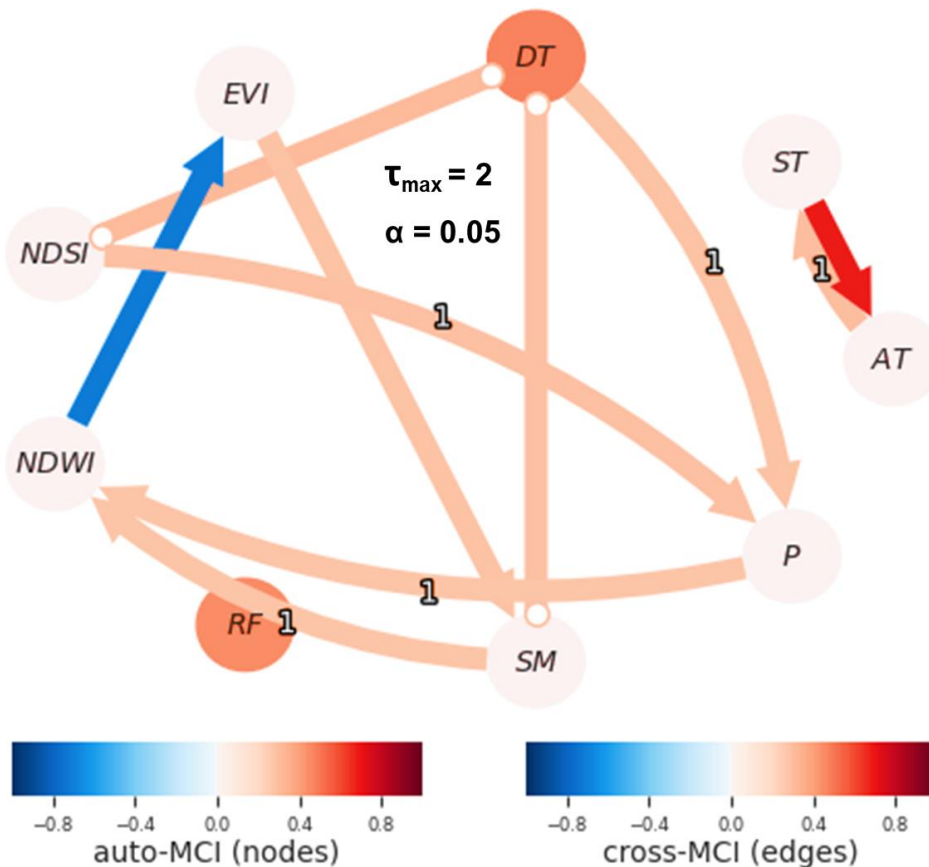
404 Fig.9 Random Forest-Regression based observed vs modeled anomalous runoff from July 1 to
405 August 31, 2022 across Upper Indus catchment as well as along all the major tributaries:

406 **4.4 Causal relationship among Hydro-climatic variables over event duration**

407 The causal analysis showed that the impact of numerous meteorological variables on the
408 extreme flood over the Upper Indus terrain varied significantly. We observed a significant
409 causal lagged connection between dewpoint temperature and NDSI, which together positively
410 influenced precipitation intensity with a 1-day lag across the Upper Indus catchment. Similarly,
411 precipitation intensity and snowmelt exhibit a positive causal influence on NDWI with a 1-day
412 lag period. For instance, the cross-correlation between precipitation and dewpoint temperature
413 with positive impact is > 0.4 over the event duration. There was a significant negative causal
414 influence of NDWI on EVI, indicating an inversely proportional relationship across the
415 observational lag period. The hydro-climatic variables such as precipitation intensity,
416 snowmelt, NDWI, EVI, NDSI, air temperature, and surface temperature, had non-linear and
417 non-stationary trends from July 1, 2022, to August 31, 2022, as shown by the autocorrelation
418 and PCMCi magnitude over the time series. The auto MCI ranges of these variables are
419 comparatively very low. Runoff and dewpoint temperatures exhibit stationarity and a linear
420 trend over the time series with relative high auto-MCI ranges. It is also observed that dewpoint
421 temperature has a significant inherent connection with snowmelt and NDSI, indicating that
422 these variables have a direct causative relationship with a high cross-MCI range (Fig. 10). In a
423 causal investigation, edges with arrows indicate a link between the drivers. However,



424 depending on the available metrics, there may be an instant causal connection between the
425 drivers. It should be observed that this relationship may not have been determined to be
426 causative.



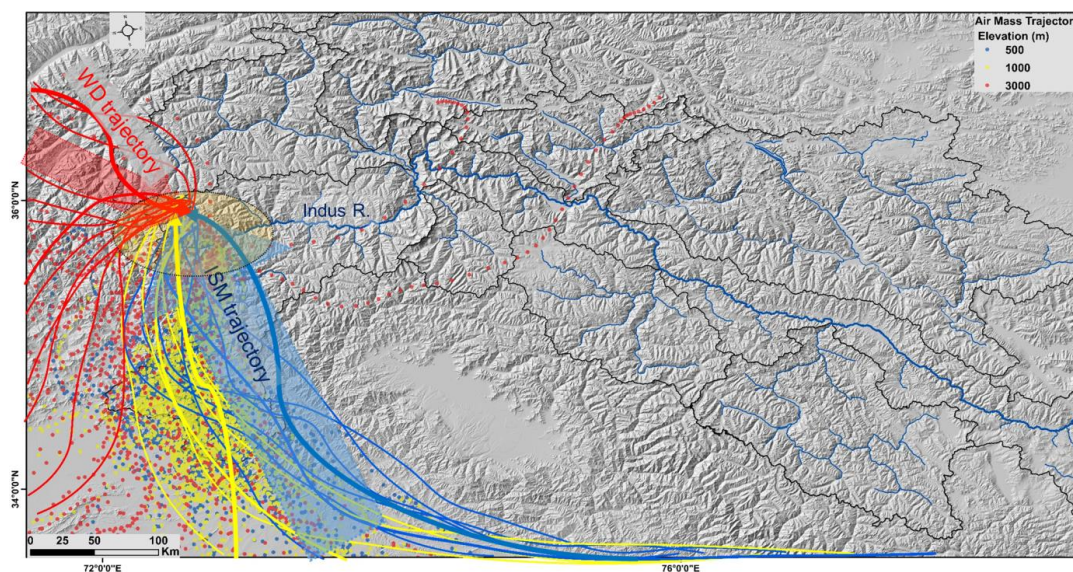
427

428 Fig.10. Causal detection among hydro-climatic driver having non-linear time series from July
429 1 to August 31, 2022 across Upper Indus catchment with maximum allowable lag of 2 days at
430 the 95% CI. (The drivers are shown in the solid circles such as: DT= Dewpoint Temperature,
431 ST= Surface Temperature, AT= Air Temperature, P= Precipitation intensity, SM= Snowmelt,
432 RF= Runoff, NDWI= Normalized Difference Water Index, NDSI= Normalized Difference
433 Snow Index, EVI= Enhanced Vegetation Index: The node colour represents autocorrelation
434 whereas link colour represents the strength of directional link. The lag at which the link was
435 found significant is shown as link label, absence of which indicates that the link was found at
436 zero lag).



437 **4.5 Identifying moisture trajectories for the anomalous precipitation event**

438 Based on moisture source uptake along trajectories for the observation period of July 1 to
439 August 31, 2022, the amount of precipitation across the orographic ridges of the Upper Indus
440 terrain was delivered along two major pathways, one from Mediterranean Sea sources such as
441 Western disturbance (WD)-derived moisture during the onset of the monsoon and a second
442 from the ISM, originating from the Bay of Bengal and the Arabian Sea. The WD routes
443 provided the moisture sources for the precipitation along the 3000 m height trajectories, while
444 the Arabian Sea, the Bay of Bengal, and the Himalayan foreland provided the moisture along
445 the 500 m and 1000 m trajectories. Furthermore, the anomalous temperature gradient observed
446 for the months of July and August 2022 shows that the steep bedrock valleys are causing
447 abnormal air-mass feedback. The substantial divergence in the air-mass curve from mid-July
448 to mid-August 2022 suggests there may have been very high precipitation and temperature
449 fluctuations during those periods (Fig. 11).



450

451 Fig.11. Moisture pathways (Backward trajectories) for Anomalous precipitation event from
452 July 1 to August 31, 2022 across Upper Indus catchment: (Blue line denotes the trajectory of
453 500 m elevation, Yellow line denotes the trajectory of 1000 m elevation, and Red line denotes
454 the trajectory of 3000 m elevation: Blue and yellow dot lines exhibits the ISM pathways,
455 whereas Red dot lines exhibit the WD pathways).

456



457 **5. Discussion**

458 **5.1 Spatial relationship between topographic metrics and event anomalies**

459 To characterize the geomorphic response of this extreme flood, we estimated stream power
460 over the trunk channel of the upper Indus River as an event anomaly. Understanding the spatial
461 distribution of stream power over the longitudinal profile of bedrock rivers is essential for
462 evaluating the catchment-scale variability in channel response to anomalous precipitation
463 events (Whipple et al., 2000; Kaushal et al., 2020). The peaks and troughs in the stream power
464 profile regulate the morphological characteristics of the bedrock channels (Schneider et al.,
465 2014; Bawa et al., 2014; Sinha et al., 2017). The river morphology and channel shape will be
466 significantly impacted by the temporal variations in flooding intensity during anomalous
467 precipitation events (Bookhagen and Strecker, 2012; Scherler et al., 2014).

468 The initial ~400–600 km length of the Upper Indus River is characterized by low gradient
469 channels as the river traverses over the elevated-low relief landscape. After traversing through
470 the mainstream and joining in the highest-order channel across the syntaxial region, there is a
471 sharp rise in the stream power profile along the downstream. The western syntax (NP-HM) in
472 the NW Himalayas is one of the most rapidly uplifting (>~5-10 mm/y) and eroding (>~10
473 mm/y) regions on earth, with extreme topographic relief (>3000 m) (Fig. 1; 2). The sudden
474 increase in the stream power of the Upper Indus River after traversing through NP-HM and the
475 resultant extreme flood along lower reaches were also attributed to this high elevation change
476 (>~4000 m) and steep channel gradient (>~20-30°) (Fig. 3b). The spatial variability of stream
477 power is also highly connected with other topographic metrics such as the k_{sn} and SL index,
478 which demonstrate a considerable rise in their longitudinal profiles when the channel crosses
479 the NP-HM region (Fig. 3a). We observed that the stream power distribution along the
480 longitudinal profiles of the Upper Indus River is characterized by numerous peaks for both
481 anomalous precipitation months in July and August 2022 (Fig. 3b).

482 The upstream glaciated channels of the Trans Himalayan and Karakoram ranges have a
483 substantial glacial influence on erosion, contributing to the main trunk channel of the Upper
484 Indus River. Therefore, such high-magnitude floods ought to propagate through the channels
485 of high mountainous tributaries like Shyok, Gilgit, and Hunza, depending on the landscape
486 characteristics of the upper Indus catchment. A moderate change in the distribution pattern of
487 snow cover may have a significant impact on glacial runoff and substantially contribute to
488 fluvial discharge. In addition to the southern mountain front, the headwaters and syntaxial zone



489 of the Upper Indus catchment received a significant amount of precipitation, which contributed
490 to the anomalous rise in stream power and substantially contributed to this extreme flood that
491 influenced the channel geometry of the lower reach and drove high bedrock erosion (Fig. 4).
492 However, the lower reaches with higher stream power are distinguished by the steep channel
493 valley and absence of sediment deposition. The observation suggests that the higher-order
494 channels of the Upper Indus River traversing across higher relief and steep gradient valleys
495 likely possess direct first-order control over the pattern of erosion when combined with an
496 anomalous rate of precipitation (Fig. 3b).

497 **5.2 Hydrological extremes and causal connections**

498 Our observations suggest that the interaction of glacial runoff with fluvial discharge over the
499 steep gradient channels combined to drive the extreme flood event across the Upper Indus
500 catchment. These extreme hydrological episodes imply that the possible response of
501 atmospheric instabilities may be elevation-dependent (Dimri et al., 2015; Forsythe et al., 2017;
502 Ullah et al., 2021; Sharma et al., 2021). It commenced with anomalous rises in temperature
503 gradients over the glaciated sub-catchments of the Upper Indus terrain, which drove the rapid
504 changes in snow cover distribution (Fig. 5; 6). This directly impacts glacial runoff magnitude
505 and contributes to an anomalous rise in fluvial stream power when traversed downstream over
506 higher-relief fluvial reaches (Fig. 6). The lower reaches of the Upper Indus catchment
507 witnessed an anomalous amount of precipitation intensity from early July to late August 2022
508 (Fig. 4).

509 When compared to the annual mean climatology, the precipitation intensity in the lower
510 reaches of the Upper Indus River was roughly ~150–200% higher in the 2022 monsoon period.
511 The moisture flux trajectories observed during the 2022 monsoonal period across the lower
512 reaches of the upper Indus River reveal two distinct sources of moisture pathways, indicating
513 that the combined effect of the westerlies-driven precipitation and the active monsoon phase
514 has likely caused this episodic event (Wang et al., 2017) (Fig. 11). Over the past years, the
515 interactions between moisture-laden ISM and southward-penetrating upper-level WD
516 depression have been linked to some catastrophic western Himalayan floods, such as in 2010
517 across Pakistan and 2013 in Uttarakhand, India (Rasmussen and Houze, 2012; Vellore et al.,
518 2015; Dimri et al., 2016; Sharma et al., 2017). This anomalous rise in the rate of precipitation
519 intensity contributes to the rapid increase in stream power across steep valleys. The combined
520 causal influence of temperature and precipitation intensity with topography plays an important



521 role in modulating such episodic events, as these variables eventually regulate the amount of
522 solid precipitation, influence the change in snow cover, and have a significant impact on
523 snowmelt runoff (Fig. 10) (Bovy et al., 2016; Godard and Tucker, 2021; Delaney et al., 2023).
524 This flood indicates the importance of understanding the cause-and-effect relationship between
525 temperature and precipitation in high-elevation uplands.

526 **5.3 Channel Response to an Extreme Flood**

527 We utilize NDWI and EVI as change indicator metrics to understand the changes in channel
528 morphology due to this extreme flood event. The spatial variability of EVI corresponds
529 significantly with an increase in NDWI intensity downstream during July and August 2022
530 (Fig. 6). This is because increasing precipitation serves a vital role in regulating relative change
531 in the EVI by decreasing surface albedo and temperature (Anderson and Goulden, 2011). In
532 some cases, correlation is due to directing flooding in vegetated areas.

533 The substantial decrease in EVI values along downstream channels has also been attributed
534 to the anomalous precipitation event, which led to increased surface runoff, higher NDWI
535 limits, and subsequent flood deposits. We observed a significant direct causal influence with
536 one-day-lagged connection of precipitation and snowmelt on NDWI (Fig. 10). This combined
537 causal relationship between precipitation and snowmelt with NDWI intensity indicates that
538 anomalous runoff occurred across both glacial and fluvial channels. Further the inverse causal
539 connection (negative MCI ranges) between NDWI and EVI illustrates the rapid change in the
540 channel geometry due to increase in the fluvial discharge over lower reaches (Fig. 10).

541 The change in river morphology driven by the high-magnitude flood episodes is also
542 documented by the statistically significant ($p < 0.005$; $R = 0.81$) relationship observed between
543 anomalous stream power and relative EVI across the lower reaches of the Upper Indus River
544 (Fig. 7). It is generally assumed that relative vegetation intensity is an indicator of geomorphic
545 change that results from short-duration, high-magnitude hydrological events (Olen et al., 2016;
546 Starke et al., 2020; Clift and Jonell, 2021; Scheip and Wegmann, 2021). Thus, we anticipate
547 that EVI acts as a spatial indicator of change in the channel morphology across the lower
548 reaches of the trunk channel during the monsoon period of 2022 (Fig. 7) suggesting that the
549 distribution of event characteristics such as NDWI and EVI can be useful to detect the relative
550 change in channel morphology triggered by high-magnitude floods.

551



552 **6. Conclusion**

553 Our study reveals several significant event characteristics of the 2022 Upper Indus flood. Our
554 analysis shows that the Upper Indus flood originated across elevated glacial channels due to
555 the anomalous temperature rise, which increased the glacial runoff. This increase in runoff
556 across glaciated catchments after traversing through fluvial reaches enhanced the fluvial
557 discharge and likely increased the stream power in the anomalous precipitation region. The
558 synoptic observation of moisture pathways indicates that this anomalous precipitation incident
559 is linked to the interaction of southward moving mid-latitude westerlies troughs and eastward
560 advancing southwestern monsoon circulation. We observe a statistically significant
561 relationship between the anomalous stream power and relative EVI change across the lower
562 reaches, which serves as a significant geomorphic indicator of change in the channel
563 morphology. This will aid in determining the reliability of EVI as a consistent indicator of
564 geomorphic changes, as well as its applicability in studying the geomorphic evolution of
565 regional landscapes. This extreme flood illustrates how causal connections between
566 temperature and precipitation across high relief-gradient channels can magnify the impacts.
567 Such hydrological events may play significant roles as efficient geomorphic agents of erosion
568 and, therefore, in the coupling of climatic extremes, topography, and erosion. This study
569 underscores the susceptibility of the elevated syntaxial region to short-lived, high-magnitude
570 flooding, indicating the need for additional research to determine the causal relationship
571 between the drivers of hydrological extremes. Significant research is needed to understand the
572 long-term impact of these extreme climatic events on the geomorphic processes in the region.

573

574

575

576

577

578

579

580



581 **Code and data availability:**

582 The Data used and methodology section includes all of the open-source datasets and tools used
583 in the study.

584 **Author contribution:**

585 Abhishek kashyap (AK): Conceptualization, Formal analysis, Methodology, writing – original
586 draft, Writing – review & editing.

587 Kristen L. Cook (KLC): Supervision, Visualization, Writing – review & editing

588 Mukunda Dev Behera (MDB): Supervision, Validation.

589 ***Competing interests**

590 The authors declare that they have no known competing financial interests or personal
591 relationships that could have appeared to influence the work reported in this paper. We wish to
592 confirm that there are no known conflicts of interest associated with this publication and there
593 has been no significant financial support for this work that could have influenced its outcome.

594 **Acknowledgments:** The authors acknowledge the authorities of IIT Kharagpur for facilitating
595 the study. AK thanks the Ministry of Education, Government of India, for the grant of a Ph.D.
596 Research Fellowship. AK thanks the IRD “South North Scheme” scholarship, managed by
597 Campus France, for the mobility and facilitation of a major part of this study at ISTERre,
598 Université Grenoble Alpes.

599

600

601

602

603

604

605

606

607

608



609 **7. References**

- 610 Adams, B.A., Whipple, K.X., Forte, A.M., Heimsath, A.M., Hodges, K.V., 2020. Climate
611 controls on erosion in tectonically active landscapes. *Sci. Adv.* 6, eaaz3166.
612 <https://doi.org/10.1126/sciadv.aaz3166>
- 613 Anderson, R.G., Goulden, M.L., 2011. Relationships between climate, vegetation, and energy
614 exchange across a montane gradient. *J. Geophys. Res.* 116, G01026.
615 <https://doi.org/10.1029/2010JG001476>
- 616 Archer, D., 2004. Hydrological implications of spatial and altitudinal variation in temperature
617 in the upper Indus basin. *Hydrology Research* 35, 209–222.
618 <https://doi.org/10.2166/nh.2004.0015>
- 619 Bawa, N., Jain, V., Shekhar, S., Kumar, N., Jyani, V., 2014. Controls on morphological
620 variability and role of stream power distribution pattern, Yamuna River, western
621 India. *Geomorphology* 227, 60–72. <https://doi.org/10.1016/j.geomorph.2014.05.016>
- 622 Benito, G., Macklin, M.G., Panin, A., Rossato, S., Fontana, A., Jones, A.F., Machado, M.J.,
623 Matlakhova, E., Mozzi, P., Zielhofer, C., 2015. Recurring flood distribution patterns
624 related to short-term Holocene climatic variability. *Sci Rep* 5, 16398.
625 <https://doi.org/10.1038/srep16398>
- 626 Bhutto, F., 2022. The west is ignoring Pakistan’s super-floods. Heed this warning: tomorrow
627 it will be you. *The Guardian*.
- 628 Bookhagen, B., Burbank, D.W., 2010. Toward a complete Himalayan hydrological budget:
629 Spatiotemporal distribution of snowmelt and rainfall and their impact on river
630 discharge. *J. Geophys. Res.* 115, 2009JF001426.
631 <https://doi.org/10.1029/2009JF001426>
- 632 Bookhagen, B., Burbank, D.W., 2006. Topography, relief, and TRMM-derived rainfall
633 variations along the Himalaya. *Geophysical Research Letters* 33, 2006GL026037.
634 <https://doi.org/10.1029/2006GL026037>
- 635 Bookhagen, B., Strecker, M.R., 2012. Spatiotemporal trends in erosion rates across a
636 pronounced rainfall gradient: Examples from the southern Central Andes. *Earth and
637 Planetary Science Letters* 327–328, 97–110.
638 <https://doi.org/10.1016/j.epsl.2012.02.005>
- 639 Bookhagen, B., Thiede, R.C., Strecker, M.R., 2005a. Abnormal monsoon years and their
640 control on erosion and sediment flux in the high, arid northwest Himalaya. *Earth and
641 Planetary Science Letters* 231, 131–146. <https://doi.org/10.1016/j.epsl.2004.11.014>



- 642 Bookhagen, B., Thiede, R.C., Strecker, M.R., 2005b. Late Quaternary intensified monsoon
643 phases control landscape evolution in the northwest Himalaya. *Geol* 33, 149.
644 <https://doi.org/10.1130/G20982.1>
- 645 Bovy, B., Braun, J., Demoulin, A., 2016. A new numerical framework for simulating the
646 control of weather and climate on the evolution of soil-mantled hillslopes.
647 *Geomorphology* 263, 99–112. <https://doi.org/10.1016/j.geomorph.2016.03.016>
- 648 Breiman, L., 2001. [No title found]. *Machine Learning* 45, 5–32.
649 <https://doi.org/10.1023/A:1010933404324>
- 650 Burbank, D.W., Anderson, R.S., 2011. *Tectonic geomorphology*. John Wiley & Sons.
- 651 Butler, R.W.H., 2019. Tectonic evolution of the Himalayan syntaxes: the view from Nanga
652 Parbat. *SP* 483, 215–254. <https://doi.org/10.1144/SP483.5>
- 653 Clift, P.D., Jonell, T.N., 2021. Monsoon controls on sediment generation and transport: Mass
654 budget and provenance constraints from the Indus River catchment, delta and
655 submarine fan over tectonic and multimillennial timescales. *Earth-Science Reviews*
656 220, 103682. <https://doi.org/10.1016/j.earscirev.2021.103682>
- 657 Cook, K.L., Andermann, C., Gimbert, F., Adhikari, B.R., Hovius, N., 2018. Glacial lake
658 outburst floods as drivers of fluvial erosion in the Himalaya. *Science* 362, 53–57.
659 <https://doi.org/10.1126/science.aat4981>
- 660 Delaney, I., Anderson, L., Herman, F., 2023. Modeling the spatially distributed nature of
661 subglacial sediment transport and erosion. *Earth Surf. Dynam.* 11, 663–680.
662 <https://doi.org/10.5194/esurf-11-663-2023>
- 663 Dimri, A.P., Chevuturi, A., Niyogi, D., Thayyen, R.J., Ray, K., Tripathi, S.N., Pandey, A.K.,
664 Mohanty, U.C., 2017. Cloudbursts in Indian Himalayas: A review. *Earth-Science*
665 *Reviews* 168, 1–23. <https://doi.org/10.1016/j.earscirev.2017.03.006>
- 666 Dimri, A.P., Niyogi, D., Barros, A.P., Ridley, J., Mohanty, U.C., Yasunari, T., Sikka, D.R.,
667 2015. Western Disturbances: A review. *Reviews of Geophysics* 53, 225–246.
668 <https://doi.org/10.1002/2014RG000460>
- 669 Dimri, A.P., Yasunari, T., Kotlia, B.S., Mohanty, U.C., Sikka, D.R., 2016. Indian winter
670 monsoon: Present and past. *Earth-Science Reviews* 163, 297–322.
671 <https://doi.org/10.1016/j.earscirev.2016.10.008>
- 672 Fadil, A., 2022. Devastating floods in Pakistan claim lives of more than 500 children.
673 UNICEF.
- 674 Farinotti, D., Immerzeel, W.W., De Kok, R.J., Quincey, D.J., Dehecq, A., 2020.
675 Manifestations and mechanisms of the Karakoram glacier Anomaly. *Nat. Geosci.* 13,



- 676 8–16. <https://doi.org/10.1038/s41561-019-0513-5>
- 677 Forsythe, N., Fowler, H.J., Li, X.-F., Blenkinsop, S., Pritchard, D., 2017. Karakoram
678 temperature and glacial melt driven by regional atmospheric circulation variability.
679 Nature Clim Change 7, 664–670. <https://doi.org/10.1038/nclimate3361>
- 680 Godard, V., Bourles, D.L., Spinabella, F., Burbank, D.W., Bookhagen, B., Fisher, G.B.,
681 Moulin, A., Leanni, L., 2014. Dominance of tectonics over climate in Himalayan
682 denudation. Geology 42, 243–246. <https://doi.org/10.1130/G35342.1>
- 683 Godard, V., Tucker, G.E., 2021. Influence of Climate-Forcing Frequency on Hillslope
684 Response. Geophysical Research Letters 48, e2021GL094305.
685 <https://doi.org/10.1029/2021GL094305>
- 686 Goodbred, S.L., Kuehl, S.A., Steckler, M.S., Sarker, M.H., 2003. Controls on facies
687 distribution and stratigraphic preservation in the Ganges–Brahmaputra delta sequence.
688 Sedimentary Geology 155, 301–316. [https://doi.org/10.1016/S0037-0738\(02\)00184-7](https://doi.org/10.1016/S0037-0738(02)00184-7)
- 689 Hack, J.T., 1973. Stream-profile analysis and stream-gradient index. Journal of Research of
690 the us Geological Survey 1, 421–429.
- 691 Hewitt, K., 2009. Catastrophic rock slope failures and late Quaternary developments in the
692 Nanga Parbat–Haramosh Massif, Upper Indus basin, northern Pakistan. Quaternary
693 Science Reviews 28, 1055–1069. <https://doi.org/10.1016/j.quascirev.2008.12.019>
- 694 Hewitt, K., 2007. Tributary glacier surges: an exceptional concentration at Panmah Glacier,
695 Karakoram Himalaya. J. Glaciol. 53, 181–188.
696 <https://doi.org/10.3189/172756507782202829>
- 697 Houze, R.A., Rasmussen, K.L., Medina, S., Brodzik, S.R., Romatschke, U., 2011.
698 Anomalous Atmospheric Events Leading to the Summer 2010 Floods in Pakistan.
699 Bulletin of the American Meteorological Society 92, 291–298.
700 <https://doi.org/10.1175/2010BAMS3173.1>
- 701 Immerzeel, W.W., Van Beek, L.P.H., Bierkens, M.F.P., 2010. Climate Change Will Affect
702 the Asian Water Towers. Science 328, 1382–1385.
703 <https://doi.org/10.1126/science.1183188>
- 704 Jaiswara, N.K., Kotluri, S.K., Pandey, A.K., Pandey, P., 2019. Transient basin as indicator of
705 tectonic expressions in bedrock landscape: Approach based on MATLAB geomorphic
706 tool (Transient-profiler). Geomorphology 346, 106853.
707 <https://doi.org/10.1016/j.geomorph.2019.106853>
- 708 Jaiswara, N.K., Kotluri, S.K., Pandey, P., Pandey, A.K., 2020. MATLAB functions for
709 extracting hypsometry, stream-length gradient index, steepness index, chi gradient of



- 710 channel and swath profiles from digital elevation model (DEM) and other spatial data
711 for landscape characterisation. *Applied Computing and Geosciences* 7, 100033.
712 <https://doi.org/10.1016/j.acags.2020.100033>
- 713 Jones, B., 2022. How melting glaciers fueled Pakistan’s fatal floods.
- 714 Joshi, S.K., Kumar, S., Sinha, R., Rai, S.P., Khobragade, S., Rao, M.S., 2023. Identifying
715 moisture transport pathways for north-west India. *Geological Journal* 58, 4428–4440.
716 <https://doi.org/10.1002/gj.4759>
- 717 Kapnick, S.B., Delworth, T.L., Ashfaq, M., Malyshev, S., Milly, P.C.D., 2014. Snowfall less
718 sensitive to warming in Karakoram than in Himalayas due to a unique seasonal cycle.
719 *Nature Geosci* 7, 834–840. <https://doi.org/10.1038/ngeo2269>
- 720 Karmouche, S., Galytska, E., Runge, J., Meehl, G.A., Phillips, A.S., Weigel, K., Eyring, V.,
721 2023. Regime-oriented causal model evaluation of Atlantic–Pacific teleconnections in
722 CMIP6. *Earth Syst. Dynam.* 14, 309–344. <https://doi.org/10.5194/esd-14-309-2023>
- 723 Kashyap, A., Behera, M.D., 2023. The influence of landslide morphology on erosion rate
724 variability across western Himalayan catchments: Role of westerlies and summer
725 monsoon interaction in the landscape characterization. *Geological Journal* gj.4913.
726 <https://doi.org/10.1002/gj.4913>
- 727 Kashyap, A., Behera, M.D., Pradhan, B., 2024. Differential surface uplift and knickpoint
728 evolution along the transient Teesta river in the eastern Himalayas. *Journal of Asian
729 Earth Sciences* 260, 105974. <https://doi.org/10.1016/j.jseaes.2023.105974>
- 730 Kaushal, R.K., Sarkar, A., Mishra, K., Sinha, R., Nepal, S., Jain, V., 2020. Spatio-temporal
731 variability in stream power distribution in the Upper Kosi River basin, Central
732 Himalaya: Controls and geomorphic implications. *Geomorphology* 350, 106888.
733 <https://doi.org/10.1016/j.geomorph.2019.106888>
- 734 Khokhar, M.N., 2022. Rich countries caused Pakistan’s catastrophic flooding. Their
735 response? Inertia and apathy. *The Guardian*.
- 736 Kirby, E., Whipple, K.X., 2012. Expression of active tectonics in erosional landscapes.
737 *Journal of Structural Geology* 44, 54–75. <https://doi.org/10.1016/j.jsg.2012.07.009>
- 738 Knox, J.C., 2000. Sensitivity of modern and Holocene floods to climate change. *Quaternary
739 Science Reviews* 19, 439–457. [https://doi.org/10.1016/S0277-3791\(99\)00074-8](https://doi.org/10.1016/S0277-3791(99)00074-8)
- 740 Koons, P., Zeitler, P., Chamberlain, C., Craw, D., Meltzer, A., 2002. Mechanical links
741 between erosion and metamorphism in Nanga Parbat, Pakistan Himalaya. *American
742 Journal of Science* 302, 749–773.
- 743 Koons, P.O., Zeitler, P., Hallet, B., 2013. Tectonic aneurysms and mountain building.



- 744 Treatise on geomorphology 5, 318–349.
- 745 Korup, O., 2012. Earth’s portfolio of extreme sediment transport events. Earth-Science
746 Reviews 112, 115–125. <https://doi.org/10.1016/j.earscirev.2012.02.006>
- 747 Korup, O., Densmore, A.L., Schlunegger, F., 2010a. The role of landslides in mountain range
748 evolution. Geomorphology 120, 77–90.
749 <https://doi.org/10.1016/j.geomorph.2009.09.017>
- 750 Korup, O., Montgomery, D.R., 2008. Tibetan plateau river incision inhibited by glacial
751 stabilization of the Tsangpo gorge. Nature 455, 786–789.
752 <https://doi.org/10.1038/nature07322>
- 753 Korup, O., Montgomery, D.R., Hewitt, K., 2010b. Glacier and landslide feedbacks to
754 topographic relief in the Himalayan syntaxes. Proc. Natl. Acad. Sci. U.S.A. 107,
755 5317–5322. <https://doi.org/10.1073/pnas.0907531107>
- 756 Kretschmer, M., Runge, J., Coumou, D., 2017. Early prediction of extreme stratospheric
757 polar vortex states based on causal precursors. Geophysical Research Letters 44,
758 8592–8600. <https://doi.org/10.1002/2017GL074696>
- 759 Krich, C., Runge, J., Miralles, D.G., Migliavacca, M., Perez-Priego, O., El-Madany, T.,
760 Carrara, A., Mahecha, M.D., 2020. Estimating causal networks in biosphere–
761 atmosphere interaction with the PCMCI approach. Biogeosciences 17, 1033–1061.
762 <https://doi.org/10.5194/bg-17-1033-2020>
- 763 Lague, D., 2014. The stream power river incision model: evidence, theory and beyond. Earth
764 Surf Processes Landf 39, 38–61. <https://doi.org/10.1002/esp.3462>
- 765 Leland, J., Reid, M.R., Burbank, D.W., Finkel, R., Caffee, M., 1998. Incision and differential
766 bedrock uplift along the Indus River near Nanga Parbat, Pakistan Himalaya, from
767 ¹⁰Be and ²⁶Al exposure age dating of bedrock straths. Earth and Planetary Science
768 Letters 154, 93–107. [https://doi.org/10.1016/S0012-821X\(97\)00171-4](https://doi.org/10.1016/S0012-821X(97)00171-4)
- 769 Leonard, J.S., Whipple, K.X., Heimsath, A.M., 2023a. Controls on topography and erosion of
770 the north-central Andes. Geology. <https://doi.org/10.1130/G51618.1>
- 771 Leonard, J.S., Whipple, K.X., Heimsath, A.M., 2023b. Isolating climatic, tectonic, and
772 lithologic controls on mountain landscape evolution. Sci. Adv. 9, eadd8915.
773 <https://doi.org/10.1126/sciadv.add8915>
- 774 Liu, P., Li, L., Guo, S., Xiong, L., Zhang, W., Zhang, J., Xu, C.-Y., 2015. Optimal design of
775 seasonal flood limited water levels and its application for the Three Gorges Reservoir.
776 Journal of Hydrology 527, 1045–1053. <https://doi.org/10.1016/j.jhydrol.2015.05.055>
- 777 Ma, Y., Hu, X., Chen, Y., Hu, Z., Feng, T., Feng, G., 2023. Different Characteristics and



- 778 Drivers of the Extraordinary Pakistan Rainfall in July and August 2022. Remote
779 Sensing 15, 2311. <https://doi.org/10.3390/rs15092311>
- 780 Montgomery, D.R., Balco, G., Willett, S.D., 2001. Climate, tectonics, and the morphology of
781 the Andes. *Geol* 29, 579. [https://doi.org/10.1130/0091-7613\(2001\)029<0579:
782 CTATMO>2.0.CO;2](https://doi.org/10.1130/0091-7613(2001)029<0579:CTATMO>2.0.CO;2)
- 783 Nanditha, J.S., Kushwaha, A.P., Singh, R., Malik, I., Solanki, H., Chuphal, D.S., Dangar, S.,
784 Mahto, S.S., Vegad, U., Mishra, V., 2023. The Pakistan Flood of August 2022:
785 Causes and Implications. *Earth's Future* 11, e2022EF003230.
786 <https://doi.org/10.1029/2022EF003230>
- 787 NDMA, 2022. NDMA monsoon 2022 daily situation report No 093.
- 788 Nowack, P., Runge, J., Eyring, V., Haigh, J.D., 2020. Causal networks for climate model
789 evaluation and constrained projections. *Nat Commun* 11, 1415.
790 <https://doi.org/10.1038/s41467-020-15195-y>
- 791 Olen, S.M., Bookhagen, B., Strecker, M.R., 2016. Role of climate and vegetation density in
792 modulating denudation rates in the Himalaya. *Earth and Planetary Science Letters*
793 445, 57–67. <https://doi.org/10.1016/j.epsl.2016.03.047>
- 794 Otto, F.E.L., Zachariah, M., Saeed, F., Siddiqi, A., Kamil, S., Mushtaq, H., Arulalan, T.,
795 AchutaRao, K., Chaithra, S.T., Barnes, C., Philip, S., Kew, S., Vautard, R., Koren, G.,
796 Pinto, I., Wolski, P., Vahlberg, M., Singh, R., Arrighi, J., Van Aalst, M., Thalheimer,
797 L., Raju, E., Li, S., Yang, W., Harrington, L.J., Clarke, B., 2023. Climate change
798 increased extreme monsoon rainfall, flooding highly vulnerable communities in
799 Pakistan. *Environ. Res.: Climate* 2, 025001. <https://doi.org/10.1088/2752-5295/acbfd5>
- 800 Panda, S., Kumar, A., Das, S., Devrani, R., Rai, S., Prakash, K., Srivastava, P., 2020.
801 Chronology and sediment provenance of extreme floods of Siang River (Tsangpo-
802 Brahmaputra River valley), northeast Himalaya. *Earth Surf Processes Landf* 45,
803 2495–2511. <https://doi.org/10.1002/esp.4893>
- 804 Piatrunia, N., 0000-0002-5341-7964, 2022. Glacial to Holocene climate variability in the
805 southern mid latitudes. <https://doi.org/10.26153/TSW/45137>
- 806 Rasmussen, K.L., Houze, R.A., 2012. A Flash-Flooding Storm at the Steep Edge of High
807 Terrain: Disaster in the Himalayas. *Bulletin of the American Meteorological Society*
808 93, 1713–1724. <https://doi.org/10.1175/BAMS-D-11-00236.1>
- 809 Ray, K., Pandey, P., Pandey, C., Dimri, A., Kishore, K., 2019. On the recent floods in India.
810 *Current science* 117, 204–218.
- 811 Rossi, M.W., Whipple, K.X., Vivoni, E.R., 2016. Precipitation and evapotranspiration



- 812 controls on daily runoff variability in the contiguous United States and Puerto Rico.
813 JGR Earth Surface 121, 128–145. <https://doi.org/10.1002/2015JF003446>
- 814 Runge, J., 2018. Causal network reconstruction from time series: From theoretical
815 assumptions to practical estimation. Chaos: An Interdisciplinary Journal of Nonlinear
816 Science 28, 075310. <https://doi.org/10.1063/1.5025050>
- 817 Runge, J., Bathiany, S., Bollt, E., Camps-Valls, G., Coumou, D., Deyle, E., Glymour, C.,
818 Kretschmer, M., Mahecha, M.D., Muñoz-Marí, J., Van Nes, E.H., Peters, J., Quax, R.,
819 Reichstein, M., Scheffer, M., Schölkopf, B., Spirtes, P., Sugihara, G., Sun, J., Zhang,
820 K., Zscheischler, J., 2019a. Inferring causation from time series in Earth system
821 sciences. Nat Commun 10, 2553. <https://doi.org/10.1038/s41467-019-10105-3>
- 822 Runge, J., Gao, P., Garcin, F., Faltings, B., 2014. Churn prediction for high-value players in
823 casual social games, in: 2014 IEEE Conference on Computational Intelligence and
824 Games. Presented at the 2014 IEEE Conference on Computational Intelligence and
825 Games (CIG), IEEE, Dortmund, Germany, pp. 1–8.
826 <https://doi.org/10.1109/CIG.2014.6932875>
- 827 Runge, J., Gerhardus, A., Varando, G., Eyring, V., Camps-Valls, G., 2023. Causal inference
828 for time series. Nat Rev Earth Environ 4, 487–505. <https://doi.org/10.1038/s43017-023-00431-y>
- 829
- 830 Runge, J., Nowack, P., Kretschmer, M., Flaxman, S., Sejdinovic, D., 2019b. Detecting and
831 quantifying causal associations in large nonlinear time series datasets. Sci. Adv. 5,
832 eaau4996. <https://doi.org/10.1126/sciadv.aau4996>
- 833 Scheip, C.M., Wegmann, K.W., 2021. HazMapper: a global open-source natural hazard
834 mapping application in Google Earth Engine. Nat. Hazards Earth Syst. Sci. 21, 1495–
835 1511. <https://doi.org/10.5194/nhess-21-1495-2021>
- 836 Scherler, D., Bookhagen, B., Strecker, M.R., 2011. Spatially variable response of Himalayan
837 glaciers to climate change affected by debris cover. Nature Geosci 4, 156–159.
838 <https://doi.org/10.1038/ngeo1068>
- 839 Schneider, J.M., Turowski, J.M., Rickenmann, D., Hegglin, R., Arrigo, S., Mao, L., Kirchner,
840 J.W., 2014. Scaling relationships between bed load volumes, transport distances, and
841 stream power in steep mountain channels: Tracer Erlenbach. J. Geophys. Res. Earth
842 Surf. 119, 533–549. <https://doi.org/10.1002/2013JF002874>
- 843 Schwanghart, W., Scherler, D., 2014. Short Communication: TopoToolbox 2 – MATLAB-
844 based software for topographic analysis and modeling in Earth surface sciences. Earth
845 Surf. Dynam. 2, 1–7. <https://doi.org/10.5194/esurf-2-1-2014>



- 846 Shahzad, F., Mahmood, S.A., Gloaguen, R., 2009. Drainage network and lineament analysis:
847 An approach for Potwar Plateau (Northern Pakistan). *J. Mt. Sci.* 6, 14–24.
848 <https://doi.org/10.1007/s11629-009-0206-4>
- 849 Sharif, M., Archer, D.R., Fowler, H.J., Forsythe, N., 2013. Trends in timing and magnitude of
850 flow in the Upper Indus Basin. *Hydrol. Earth Syst. Sci.* 17, 1503–1516.
851 <https://doi.org/10.5194/hess-17-1503-2013>
- 852 Sharma, S., Sati, S.P., Basavaiah, N., Pandey, S., Sundriyal, Y.P., Rana, N., Singh, P.,
853 Pradhan, S., Shukla, A.D., Bhushan, R., Bhatt, R., Juyal, N., 2022. Mid to late
854 Holocene climate variability, forest fires and floods entwined with human occupation
855 in the upper Ganga catchment, India. *Quaternary Science Reviews* 293, 107725.
856 <https://doi.org/10.1016/j.quascirev.2022.107725>
- 857 Sharma, S., Shukla, A.D., Bartarya, S.K., Marh, B.S., Juyal, N., 2017. The Holocene floods
858 and their affinity to climatic variability in the western Himalaya, India.
859 *Geomorphology* 290, 317–334. <https://doi.org/10.1016/j.geomorph.2017.04.030>
- 860 Sinha, R., Mohanta, H., Jain, V., Tandon, S.K., 2017. Geomorphic diversity as a river
861 management tool and its application to the Ganga River, India. *River Research &*
862 *Apps* 33, 1156–1176. <https://doi.org/10.1002/rra.3154>
- 863 Snyder, N.P., Whipple, K.X., Tucker, G.E., Merritts, D.J., 2003. Importance of a stochastic
864 distribution of floods and erosion thresholds in the bedrock river incision problem. *J.*
865 *Geophys. Res.* 108, 2001JB001655. <https://doi.org/10.1029/2001JB001655>
- 866 Srivastava, P., Kumar, A., Chaudhary, S., Meena, N., Sundriyal, Y.P., Rawat, S., Rana, N.,
867 Perumal, R.J., Bisht, P., Sharma, D., Agnihotri, R., Bagri, D.S., Juyal, N., Wasson,
868 R.J., Ziegler, A.D., 2017. Paleofloods records in Himalaya. *Geomorphology* 284, 17–
869 30. <https://doi.org/10.1016/j.geomorph.2016.12.011>
- 870 Starke, J., Ehlers, T.A., Schaller, M., 2020. Latitudinal effect of vegetation on erosion rates
871 identified along western South America. *Science* 367, 1358–1361.
872 <https://doi.org/10.1126/science.aaz0840>
- 873 Tibau, X.-A., Reimers, C., Gerhardus, A., Denzler, J., Eyring, V., Runge, J., 2022. A
874 spatiotemporal stochastic climate model for benchmarking causal discovery methods
875 for teleconnections. *Environ. Data Science* 1, e12. <https://doi.org/10.1017/eds.2022.11>
- 876 Vellore, R.K., Kaplan, M.L., Krishnan, R., Lewis, J.M., Sabade, S., Deshpande, N., Singh,
877 B.B., Madhura, R.K., Rama Rao, M.V.S., 2016. Monsoon-extratropical circulation
878 interactions in Himalayan extreme rainfall. *Clim Dyn* 46, 3517–3546.
879 <https://doi.org/10.1007/s00382-015-2784-x>



- 880 Wang, N., Zeng, X.-M., Guo, W.-D., Chen, C., You, W., Zheng, Y., Zhu, J., 2018.
881 Quantitative diagnosis of moisture sources and transport pathways for summer
882 precipitation over the mid-lower Yangtze River Basin. *Journal of Hydrology* 559,
883 252–265. <https://doi.org/10.1016/j.jhydrol.2018.02.003>
- 884 Whipple, K.X., Hancock, G.S., Anderson, R.S., 2000. River incision into bedrock: Mechanics
885 and relative efficacy of plucking, abrasion, and cavitation. *Geological Society of
886 America Bulletin* 112, 490–503. [https://doi.org/10.1130/0016-
887 7606\(2000\)112<490:RIIBMA>2.0.CO;2](https://doi.org/10.1130/0016-7606(2000)112<490:RIIBMA>2.0.CO;2)
- 888 Whipple, K.X., Tucker, G.E., 1999. Dynamics of the stream-power river incision model:
889 Implications for height limits of mountain ranges, landscape response timescales, and
890 research needs. *J. Geophys. Res.* 104, 17661–17674.
891 <https://doi.org/10.1029/1999JB900120>
- 892 Wobus, C., Whipple, K.X., Kirby, E., Snyder, N., Johnson, J., Spyropolou, K., Crosby, B.,
893 Sheehan, D., 2006. Tectonics from topography: Procedures, promise, and pitfalls, in:
894 Tectonics, Climate, and Landscape Evolution. Geological Society of America.
895 [https://doi.org/10.1130/2006.2398\(04\)](https://doi.org/10.1130/2006.2398(04))
- 896 Wolfensberger, D., Gabella, M., Boscacci, M., Germann, U., Berne, A., 2021. RainForest: a
897 random forest algorithm for quantitative precipitation estimation over Switzerland.
898 *Atmos. Meas. Tech.* 14, 3169–3193. <https://doi.org/10.5194/amt-14-3169-2021>
- 899 Wu, K., Liu, S., Jiang, Z., Liu, Q., Zhu, Y., Yi, Y., Xie, F., Ahmad Tahir, A., Saifullah, M.,
900 2021. Quantification of glacier mass budgets in the Karakoram region of Upper Indus
901 Basin during the early twenty-first century. *Journal of Hydrology* 603, 127095.
902 <https://doi.org/10.1016/j.jhydrol.2021.127095>
- 903 Zeitler, P.K., Koons, P.O., Bishop, M.P., Chamberlain, C.P., Craw, D., Edwards, M.A.,
904 Hamidullah, S., Jan, M.Q., Khan, M.A., Khattak, M.U.K., Kidd, W.S.F., Mackie,
905 R.L., Meltzer, A.S., Park, S.K., Pecher, A., Poage, M.A., Sarker, G., Schneider, D.A.,
906 Seeber, L., Shroder, J.F., 2001. Crustal reworking at Nanga Parbat, Pakistan:
907 Metamorphic consequences of thermal-mechanical coupling facilitated by erosion.
908 *Tectonics* 20, 712–728. <https://doi.org/10.1029/2000TC001243>
- 909 Zeitler, P.K., Meltzer, A.S., Brown, L., Kidd, W.S., Lim, C., Enkelmann, E., 2014. Tectonics
910 and topographic evolution of Namche Barwa and the easternmost Lhasa block, Tibet,
911 in: *Toward an Improved Understanding of Uplift Mechanisms and the Elevation
912 History of the Tibetan Plateau*. Geological Society of America Special Papers, pp. 23–
913 58.